pure component properties, thus eliminating the necessity of any experimental data. The predicted γ values are comparable to those obtained from data reported in the literature. The present study has been limited to γ^{∞} less than 1.65. However, the proposed method inherits the limitations of the Wilson equation.

Acknowledgment

Thanks are due to the management of Engineers India Ltd. for permission to publish the present work.

Nomenclature

g^E = Gibbs excess free energy, cal/mol
i,j = any component, $l \neq j$
A_{ji} = constant
x_i = liquid phase concentration, mole fraction
V_i = molar volume, cm^3/mol
g_{ij} = interaction parameter between unlike molecules
g_{12}^1, g_{12}^2 = constants as defined by eq 2a and 2b
g_{ii} = interaction parameter between like molecules
γ_i = activity coefficient at finite dilution
γ_i^{∞} = activity coefficient at infinite dilution
R = universal gas constant, cal/mol °K
T = temperature, °K
δ_i = solubility parameter, $(cal/cm^3)^{1/2}$
A,B,C,D = constants
λ_{ij} = constant in single parameter equation as used by Eckert

Literature Cited

Bruin, S., *Ind. Eng. Chem., Fundam.*, **9**, 305 (1970).
Bruin, S., Prausnitz, J. M., *Ind. Eng. Chem., Process Des. Dev.*, **10**, 562 (1971).
Flory, P. J., *J. Chem. Phys.*, **9**, 660 (1941); **10**, 51 (1942).
Hala, E., *AIChE J.*, **18**, 876 (1972).
Hala, E., Wichterle, I., Polak, J., Boublik, T., "Vapour Liquid Equilibrium Data at Normal Pressures," pp 24–441, Pergamon Press, London, 1968.
Hankinson, R. W., Langfitt, B. D., Tassios, D. P., *Can. J. Chem. Eng.*, **50**, 511 (1972).
Heil, J. F., Prausnitz, J. M., *AIChE J.*, **12** (4), 678 (1966).
Huggins, M. L., *J. Phys. Chem.*, **9**, 440 (1941).
Huggins, M. L., *Ann. N.Y. Acad. Sci.*, **43**, 1 (1942).
Lange, N. A., "Handbook of Chemistry," pp 404–741, 1506–1510, McGraw-Hill, New York, N.Y., 1967.
Lydersen, A. L., cf. "The Properties of Gases and Liquids," p 8, R. C. Reid and T. K. Sherwood, Ed., McGraw-Hill, New York, N.Y., 1966.
McKelvey, F. E., *Hydrocarbon Process. Pet. Refiner.*, **43** (5), 145 (1964); **43** (6), 147 (1964).
Orye, R. V., Prausnitz, J. M., *Ind. Eng. Chem.*, **57**, (5), 18 (1965).
Riedel, L., *Z. Elektrochem.*, **53**, 222 (1949).
Schreiber, L. B., Eckert, C. A., *Ind. Eng. Chem., Process Des. Dev.*, **10**, 572 (1971).
Tassios, D., presented at the 62nd Annual meeting of AIChE, Washington, D.C., Nov 1969.
Tassios, D., *AIChE J.*, **17** (6), 1367 (1971).
Wilson, G. M., *J. Am. Chem. Soc.*, **86**, 127 (1964).

Received for review March 29, 1974
Accepted January 2, 1975

The Kinetics of Gasification of Carbon Contained in Coal Minerals at Atmospheric Pressure

G. A. Jensen

Washington State University, Pullman, Washington 99163

Coal minerals obtained from Kentucky No. 9 coal were studied experimentally for the kinetics of carbon removal by reaction with steam. A batch fluid bed reactor was operated at temperatures between 1040 and 1430°C to produce synthesis gas (CO + H_2). Sulfides in the coal minerals were converted to hydrogen sulfide during gasification. The carbon–steam reaction was slow, reaction rate controlled, and the reaction rate was independent of particle size. The shrinking core model approximates the kinetics of the reaction.

Commercial-scale solvent refining of coal will begin soon. Coal, when solvent refined, requires reaction with hydrogen to liquefy the contained carbonaceous matter. The products are a meltable solid, gases, and a carbon- and mineral-containing residue. The residue is not an ash because it has been subjected only to reducing conditions and not to high-temperature oxidation; it is referred to as coal minerals. Table I shows typical analysis of coal minerals produced from several coals (Kloepper et al., 1965). The loss on ignition is nearly all carbon.

Synthesis gas can be produced by reacting the carbon in coal minerals with steam and after sulfur removal can be used to supply hydrogen for solvent refining coal. The kinetics of the carbon–steam reaction in coal minerals was therefore studied to characterize the reaction rate-controlling mechanism. Synthesis gas produced by gasification of the carbon in the Kentucky No. 9 coal mineral residue used in this study is in excess of the solvent refined coal processing requirements.

Previous Work

Retorted coal minerals from the solvent refining process have negligible volatile content and a reactivity near that of petroleum coke or calcined anthracite. Lowry (1947a,b, 1963) has reviewed the extensive literature on the gasification of similar materials. The following reactions are significant at atmospheric pressure.

$$C + H_2O \longrightarrow CO + H_2 \quad (1)$$

$$CO + H_2O \longrightarrow CO_2 + H_2 \quad (2)$$

Reaction 1 goes to completion above 870°C. CO_2 production is usually small because the equilibrium constant for reaction 2 is two orders of magnitude below that for reaction 1. Steam decomposition via reaction 1 is determined by residence time and reaction rate. Equilibrium for the formation of methane and other possible carbon–steam reactions is not favored at atmospheric pressure. Methane formation and other reactions therefore will be minimal.

Table I. Analysis of Coal Minerals for Representative United States Coals

Component	Kentucky Sample 57215, %	West Virginia Sample 57244, %	North Dakota Lignite Sample 57250, %	Washington Sample 57263, %	Wyoming Sample 57264, %
Ignition loss	55.23	34.64	65.16	26.9	81.0
SiO_2	18.42	28.95	12.50	37.9	9.56
Al_2O_3	10.07	14.19	5.49	4.84	1.79
Fe_2O_3	10.55	16.45	3.13	23.62	5.08
TiO_2	0.20	0.57	0.11	0.87	0.10
MgO	1.66	1.46	2.36	1.73	0.41
CaO	1.09	1.85	4.45	1.56	0.61
K_2O	1.13	0.70	0.25	0.42	0.08
Na_2O	0.78	0.52	1.18	0.48	0.10
B_2O_3	0.21	0.19	0.09	0.05	0.06
CuO	0.62	0.038	0.018	0.04	0.007
V_2O_5	0.066	0.057	0.016	0.054	0.004
ZrO_2	0.068	0.081	0.033	0.03	0.02
BaO	0.074	0.067	0.31	0.21	0.06
MnO	0.035	0.032	0.065	0.01	0.004
PbO	0.022	0.018	0.008	0.026	0.008
SrO	0.027	0.047	0.100	0.36	0.08
NiO	0.027	0.020	0.005	0.009	0.002
Cr_2O_3	0.024	0.025	0.006	0.014	0.003
CoO	0.015	0.013	0.006	0.003	0.002
MoO_3	0.014	0.005	0.004	...	0.001
Ga_2O_3	0.012	0.011	0.006	0.008	0.001
SnO	0.004	0.005	0.0015	...	0.0006
Ag_2O	0.0004	0.0003	0.0005	0.0001	0.0001
GeO_2	...	...	...	...	0.005

Earlier kinetic studies of the reaction of several forms of carbon with steam have reported reaction 1 as zero order (Scott, 1941), fractional and first order (Gadsby et al., 1948; Haslam et al., 1923; Key et al., 1930) and between first and second order (Key et al., 1930; Scott, 1941) with respect to steam.

Much of the work prior to 1960 has not been reported in a form which makes direct comparisons possible. Levenspiel (1967), Wen (1968), Ishida and Wen (1968, 1971) have developed general mathematical models for comparing pilot plant data. Some experimental data using mathematical models are available (Wen, 1962).

Experimental Apparatus

Jensen (1968–1972) and Vohra (1972) showed that coal minerals in fixed bed reactors tended to fuse. A batch fluid bed reactor was selected for this work because solids reacting in fluid beds have less tendency to agglomerate. A flow diagram of the reactor system used is shown in Figure 1.

The reactor consisted of three sections: a stainless steel expanded disengaging section to knock back entrained dust, a 2-in. diameter by 1 ft long heated section contained in a gas-fired furnace, and a heated steel bottom section for vaporization of water with a removable porous stainless steel bed support and gas distributor. Asbestos rope was used as a packing to form gas-tight seals between the ceramic and stainless steel reactor parts. Distilled water was fed through a calibrated rotameter and volatilized to steam in the lower part of the apparatus. The product gases passed through a small heated cyclone, a condenser, a cold trap, a soap bubble flowmeter, and were then exhausted. Gas samples were obtained directly from the effluent gas by drawing a sample stream through a Carle sampling valve which injected samples directly into the carrier gas of the gas chromatograph. Additional intermediate samples were taken using gas-tight syringes.

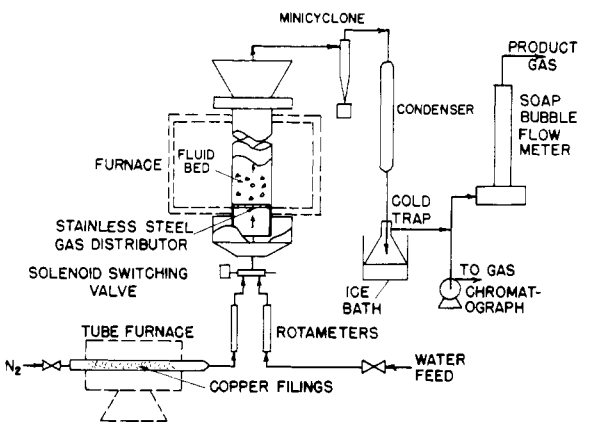

Figure 1. Flow diagram of experimental apparatus.

Coal Mineral Preparation

As received, the Kentucky No. 9 minerals were lumps up to ½ in. in diameter. The lumps were ground to pass 20-mesh with an attrition or ball mill, then sieved for experiments. The fractions used were 30/35-mesh (0.50–0.59 mm), 50/60-mesh (0.21–0.30 mm) and 200/270-mesh (0.05–0.07 mm).

Procedure

A reactor charge of 100 g of coal minerals was fed to the cold reactor. Nitrogen was used as a fluidizing gas during warmup to prevent oxidation and to keep the bed fluid and avoid slugging when steam was introduced. Nitrogen flow was stopped and steam was passed through the bed when the reactor reached the experimental reaction temperature.

A total radiation pyrometer measured the reactor temperature. It was impossible to measure the bed temperature, for a fine black dust constantly obscured it. Reactor

temperatures therefore were measured at the exterior reactor surface. Initial manual control and subsequent automatic burner control held the reactor surface to ±25° of the selected reaction temperature. Reaction temperatures were 1040, 1150, and 1320°C.

The minimum steam flow rate for fluidizing the bed was determined by cold test in a Lucite model using air or hydrogen as a fluidizing gas. The fluid bed height for 100 g of coal minerals was 7 in. A minimum gas rate of 20 l./min was required for fluidization. Entrainment losses did not exceed 5% under the conditions used and averaged 2%. Calculation showed that a satisfactory steam rate above 24 l./min could be obtained using a water rate of 4 ml/min. At the completion of an experiment, nitrogen was again introduced and continued throughout the cooling period to prevent oxidation of any free iron formed.

Analytical

Analysis of the gases for hydrogen sulfide, carbon dioxide, hydrogen, carbon monoxide, water, oxygen, nitrogen, sulfur dioxide, and carbonyl sulfide was by means of gas chromatography. Loss of COS and H_2S in the cold traps was checked during early experiments and considered nil. The usual procedure for analysis of gases of this type requires a separate analysis for hydrogen (Jones, 1967, Purcell and Ettre, 1965). When helium is used as a carrier gas, the thermal conductivity detectors which were used to detect hydrogen are not suitable. Purcell and Ettre (1965) suggested the use of an 8.5% hydrogen, 91.5% helium carrier gas. Jones (1967) used a dual column with back flushing. Minor modifications of both procedures provided a system which functioned well and did not require back flushing.

A Porapak Q-S column separated carbon dioxide, hydrogen sulfide, water, sulfur dioxide, and the other larger or polar compounds from the gases. A molecular sieve (13x + 5A) separated hydrogen, nitrogen, oxygen, methane, and carbon dioxide. The chromatographic columns were prepared and mounted in a Varian Model 1800 dual-column gas chromatograph. Carle sampling valves switched the samples directly into the mixed carrier gas. The lighter nonpolar compounds (H_2, CO, N_2, O_2, CH_4) passed rapidly through the Porapak Q-S column as a single peak and entered the molecular sieve column. This column was then switched out of the eluting gas stream and the analysis of the materials on the Porapak completed as usual. The molecular sieve column was then switched back into the stream and its contents determined. The Porapak column temperature was programmed to rise from 45 to 210°C at 15°/min after hydrogen had eluted from the apparatus. The molecular sieve column was simply heated from ambient to approximately 100°C as rapidly as the Beckman Thermotrack oven would heat, approximately 5 min. Elution time was consistent using this method of heating.

Experimental Results

At 1150 and 1320°C, carbon monoxide and hydrogen were the major products of the reaction. CO_2 concentrations were under 2% during the early stages of the reaction and increased with time. At 1040°C, CO_2 replaced CO as a major product, the CO/CO_2 ratio increasing with time; H_2 remained constant. The rate of gas evolution decreased steadily throughout each experiment. Hydrogen sulfide increased slowly, peaked, then rapidly dropped off. Hydrogen sulfide, methane, carbonyl sulfide, and nitrogen ordinarily totaled under 4% of the gas mix. Residues after reaction were either hard and slag-like masses or powders similar to the charge. Some slags contained iron metal inclusions.

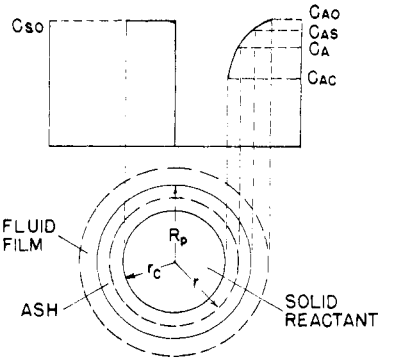

Figure 2. Schematic diagram of concentration profile for the unreacted shrinking core model.

Discussion of the Carbon–Steam Reaction

The rate of chemical reaction 1 is

$$-ak_vC_AC_S = ak_SC_AC_S = M_A \qquad (3)$$

assuming only CO and hydrogen are evolved. Carbon dioxide, which appears late in experiments above 1150° and throughout experiments at 1040°, must result from the shift reaction 2. May et al. (1958) suggest that the forward rate of the shift reaction is slower than the carbon–steam reaction rate and decreases with temperature. The equilibrium constant for the shift reaction 2 also decreases with temperature (Lowry, 1963). The shift reaction initially is not significant on the particle surface because of its lower rate, so the CO concentration is quite high. As carbon is removed and the thickness of the ash layer increases, there is more residence time for the steam and carbon monoxide to interact as they diffuse through the ash layer, permitting the shift reaction to occur and to form more carbon dioxide. Some of the ash constituents are known accelerating catalysts for the shift reaction. Larger particles should show the increase in carbon dioxide concentration sooner than small particles if the rate process is not independent of particle size. This effect is obscured by the tendency of the minerals to melt above 1100° when their carbon content has become low. Below 1100°, the forward rate of the shift reaction decreases at a rate lower than the carbon–steam reaction; thus carbon dioxide would appear sooner in the gas phase. Our observations confirm this.

The kinetic analysis assumes that reaction 1 is most important. Carbon dioxide is all made by reaction 2. The sum of CO + CO_2 thus represents the conversion of carbon in the bed. The unreacted shrinking core model of Levenspiel (1967) as modified by Ishida, Wen and coworkers (1968, 1971) was used for data analysis. Their publications give the complete mathematical analysis, and only those relationships required for use here are repeated for convenience. Figure 2 shows the concentration profile for the unreacted shrinking core model. A material balance yields

$$\epsilon\frac{\partial C_A}{\partial t} = D_{eA}\left\{\frac{\partial^2 C_A}{\partial r^2} + \frac{2}{r}\frac{\partial C_A}{\partial r}\right\} \quad R_p > r > r_c \qquad (4)$$

D_{eA} is the effective diffusion coefficient for component A through the ash layer. Assumptions involved in deriving eq 4 are (a) diffusion of component A is through a spherical shell of thickness r, (b) diffusion rate is independent of concentration, and (c) chemical reaction occurs only at the surface of the shrinking core.

The boundary conditions are: (1) at the particle surface R_p

$$D_{eA}\left[\frac{\partial C_A}{\partial r}\right]_{R_\rho} = k_{mA}(C_{Ao} - C_{AS}) \quad (5)$$

and (2) at the moving surface r_c

$$D_{eA}\left[\frac{\partial C_A}{\partial r}\right]_{r_c} = ak_S C_{So} C_{Ao} \quad (6)$$

but since the surface is continually changing with time

$$-D_{eA}\left[\frac{\partial C_A}{\partial r}\right]_{r_c} = aC_{So}\left[\frac{\partial r_c}{\partial t}\right] \quad (7)$$

The initial condition is $r_c = R_\rho$ at $t = 0$. A pseudo-steady state is assumed to exist within the particle relative to the concentration of component A, so

$$\epsilon\frac{\partial C_A}{\partial t} = 0 \quad (8)$$

Wen (1968) has integrated eq 4 with the given boundary conditions. Using simplifying assumptions, he shows for materials reacting at the shrinking core surface, when ash film resistance is controlling

$$t = \frac{aC_{So}R^2}{2C_{Ao}D_{eA}}[1 - (1 - X)^{1/3}]^2 \quad (9)$$

and for chemical reaction rate controlling

$$t = \frac{R}{k_S C_{Ao}}[1 - (1 - X)^{1/3}] \quad (10)$$

For particles of unchanging size, the time needed for the same conversion is

$$t \propto R^2 \text{ (for ash film controlling)} \quad (11)$$

$$t \propto R \text{ (for chemical reaction controlling)} \quad (12)$$

A plot of log t vs. $[1 - (1 - X)^{1/3}]$ thus permits a determination of the rate-controlling factor. A slope of 1 indicates chemical reaction controls and a slope of 2 that diffusion controls. When chemical reaction is slow and diffusion is rapid, the concentration of component A at the reacting surface will be nearly that in the bulk stream.

$$C_A = C_{Ao} \text{ for } 0 < r < R_\rho \quad (13)$$

$$\frac{C_S}{C_{So}} = 1 - X \text{ where } X = \frac{t_v}{t_v^*} \quad (14)$$

Equations 13 and 14 imply that the concentration of the solid reactant, not the particle diameter, governs the conversion, so

$$t_v \propto R^0 \quad (15)$$

The time for complete conversion is thus independent of the original particle size. Wen (1968) also shows that the relation between X and t_v/t_v^* for the general, homogeneous, and shrinking core models for chemical reaction rate controlling has the same form. The equations relating the controlling step to reaction time are thus valid using either the general or unreacted shrinking core models, but do not predict the mechanism if the rate of reaction is independent of particle size. Additional data are necessary to clarify the reaction mechanisms.

Wen (1968) suggested the use of an effectiveness factor η for this purpose.

$$\eta = \frac{\text{(actual reaction rate)}}{\text{reaction rate obtainable at the concentration and temperature of the bulk phase}} = \frac{\int k_r C_S C_A \, dV}{\int k_r C_{So} C_{Ao} \, dV} \quad (16)$$

This effectiveness factor relates the reaction rate at any instant to the initial rate and permits examination of the effect of diffusion. Wen, Ishida et al. (1971) plot theoretically derived curves to demonstrate the effect of ash diffusion and fluid film resistance on the solid-fluid reaction. Plots of conversion and effectiveness factors against time permit determination of the rate-controlling step and a general model from pilot plant data.

The raw data were plotted as carbon gasification rate vs. time and graphically integrated to obtain carbon conversions. Carbon conversions vs. time are shown in Figures 3, 4, 5, and 6 plotted as t vs. $1 - (1 - X)^{1/3}$. The slope of the lines obtained ranged from 0.89 to 1.14 (cf. Table II) and averaged 1.0, showing that the reaction is probably controlled by the first-order reaction rate. When curvature toward horizontal occurs, melting or sintering in the fluid bed has occurred.

For a rate-controlled solid-fluid reaction, the intercept represents $R/k_S C_A$. At a particular temperature, k_S and C_A are constant for the reaction, so changes in the intercepts should show the effect of particle size on reaction rate. No trend is observed in the data of Table II so the reaction is believed to be independent of particle size. If particle size does not influence the reaction rate, diffusion of the reacted material must be rapid and rate of chemical reaction slow and controlling. Unfortunately, under these conditions, the selection between homogeneous and shrinking core models from experimental data is difficult.

Samples carefully sized within a narrow range of particle sizes and others with a wide range were compared, for if the results were identical this would confirm that reaction rate was independent of particle size. The slopes of the curves obtained from the unsieved samples are the same as those from sieved samples, but the intercepts are higher (cf. Table II). The results of the rate data from these runs are confusing and it is believed that internal melting, which would lower the diffusion rate without affecting the reaction rate, may be the cause of the anomalies.

The effectiveness factor is proportional to the reaction rate per unit reaction surface area. Reaction rate per unit reaction surface area is defined as

$$(n_s)_{\bar{r}_c} \propto \frac{M_A}{4\bar{r}_c^2} \quad (17)$$

where $\bar{r}_c$ is defined (Ishida et al., 1971) as

$$4\pi\bar{r}_c^2 = 4\pi R^2(\bar{r}_c/R)^2 = 4\pi R^2(1 - X)^{2/3} \quad (18)$$

Normalizing by dividing by the reaction rate per unit reaction surface area at $X = 0$, unit reaction rates were calculated and plotted in Figures 7, 8, 9, and 10 vs. carbon conversion to attempt a clarification of the mathematical model.

The data for coal minerals gasified at 1040°C all show a sharp downward curvature after 30–50% carbon removal in Figures 7 and 10. Wen et al. (1962) observed that the carbon in char had a variable reactivity. The carbon in coal minerals can be assumed to have a similar character and may contain graphite, char, and other forms of carbon. Surface area per unit mass is inversely proportional to particle size. The carbon contained in the smallest particles may have a greater concentration of the more graphitic, unreactive carbon species than either the intermediate or large size particles; thus, the carbon-steam reaction would continue until the reactive carbon was removed, leaving the unreacted carbon virtually untouched. The large particles, although they have a larger quantity of active carbon species, are surface area limited. Unless enough reactive carbon is removed by the reaction at the

Table II. Slope and Intercept of ln $[1 - (1 - X)^{1/3}]$ vs. t, Carbon Gasification

	Particle size–mm							
	0.50–0.59		0.21–0.59		0.05–0.07		Ground coal minerals	
Temp, °C	Slope	Intercept	Slope	Intercept	Slope	Intercept	Slope	Intercept
1040	0.98	0.0021	1.06	0.0023	0.89	0.0024	0.91	0.0079
1150	1.00	0.0111	0.95	0.0109	1.01	0.0084	0.91	0.0912
1320	0.98	0.0058	1.14	0.0060	1.13	0.0055	1.03	0.0138

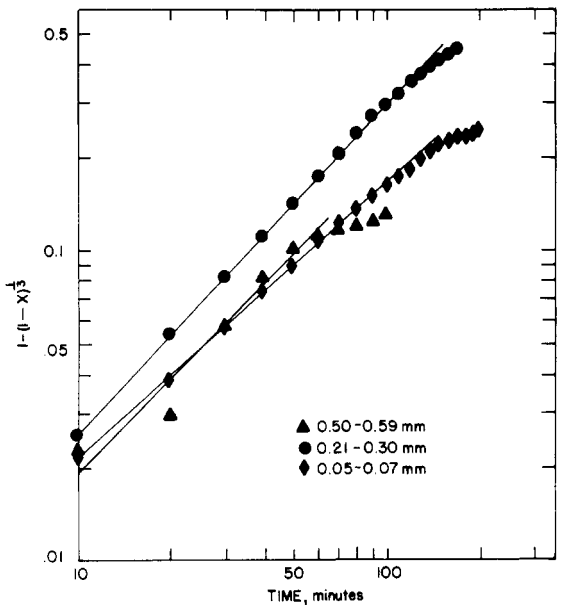

Figure 3. Kinetic model, steam reacting with the carbon contained in coal minerals at 1040°C.

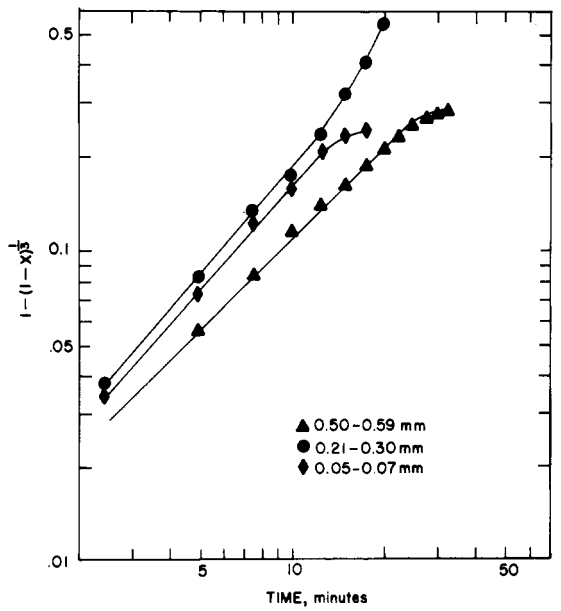

Figure 5. Kinetic model, steam reacting with the carbon contained in coal minerals at 1320°C.

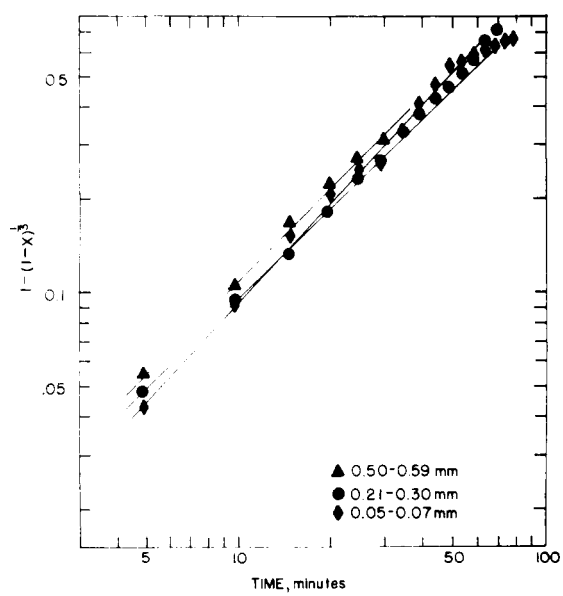

Figure 4. Kinetic model, steam reacting with the carbon contained in coal minerals at 1150°C.

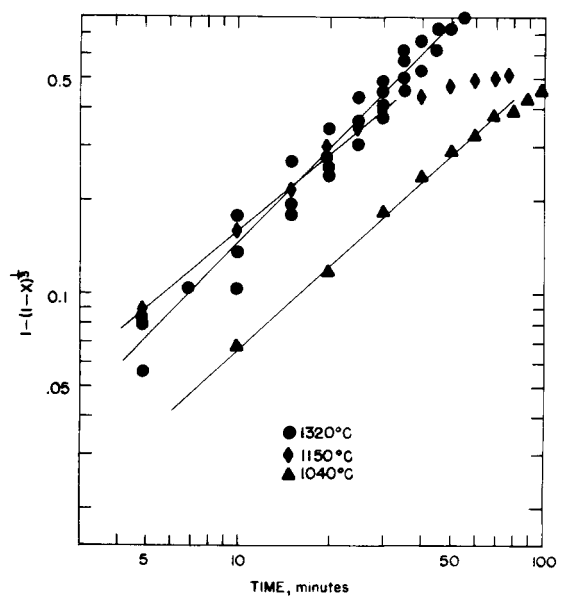

Figure 6. Kinetic model, steam reacting with the carbon contained in coal minerals, unsieved, ground coal minerals.

surface of the largest particle to open passageways for diffusion through the carbon-ash matrix, the reaction would appear completed after only the surface layers of carbon are removed. The intermediate size particles probably have sufficient surface and enough reactive carbon species to account for the greater carbon conversion.

At 1150°C (Figure 8 and Figure 10) for ground but not sieved coal minerals, a horizontal line results showing that the reaction is essentially rate controlled to over 80% carbon conversion. No significant deviation from the horizontal is observed except that a slight drop in the intermediate particle data is observed at about 70% conversion. Some internal particle melting may have occurred during this experiment. These results suggest that the optimum temperature range for the gasification of the carbon in coal minerals may be 1100-1200°C. Most of the carbon

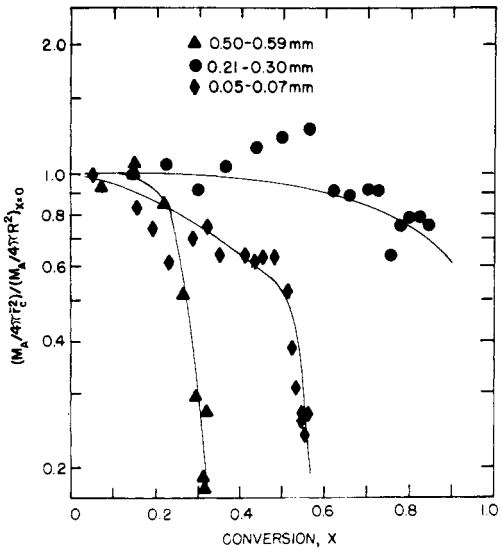

Figure 7. Reaction rate per unit reaction surface area, carbon-steam reaction at 1040°C.

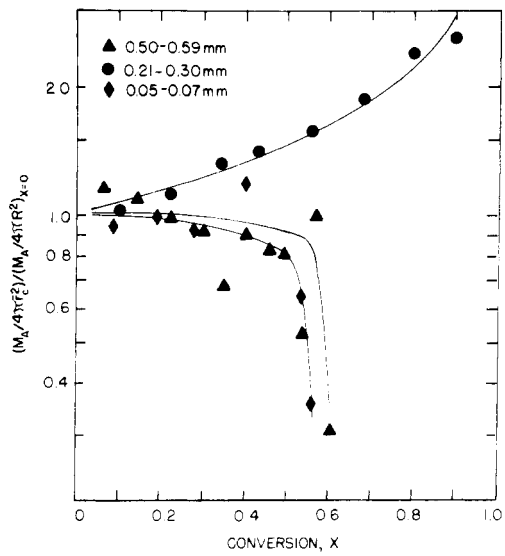

Figure 9. Reaction rate per unit reaction surface area, carbon-steam reaction at 1320°C.

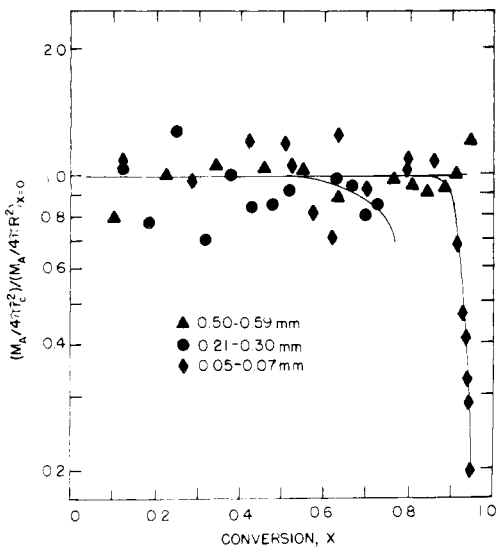

Figure 8. Reaction rate per unit reaction surface area, carbon-steam reaction at 1150°C.

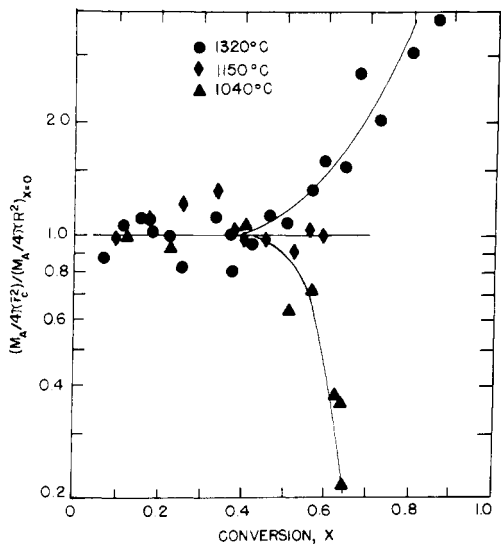

Figure 10. Reaction rate per unit reaction surface area, carbon-steam reaction, unsieved, ground coal minerals.

species are probably reactive and melting of the minerals within the particles does not occur.

Deviations in the high temperature 1320°C runs are primarily caused by the melting characteristics of the ash-forming constituents in the coal minerals. Softening of coal ash begins at approximately 1200°C and ash may be quite fluid at 1300°C. Samples of coal minerals were heated to 1800°C in an inert atmosphere but melting did not occur. Synthetic coal mineral mixtures deficient in carbon melted at temperatures as low as 1200°C (Jensen, 1968–1972). Melting temperature was proportional to carbon content up to 40% carbon. Melting and sinter formation were observed after completion of all experiments at 1320°C. The larger particles were generally sintered while small particles tended to fuse. Sinter formation was greater where large particles were present and may have occurred during furnace warm up. The larger particles which were generally lower in carbon content had sufficient size so that only minimal surface would exist at points of contact between particles. Fusion at the points of contact would not result in a strong bond between the particles and weak sintered edges would be continually broken up by the fluidizing action of the steam creating new carbon surface for reaction. Pore size of the sinter would also be increasing, exposing new carbon surface and increasing the reaction rate per equivalent reaction surface. The rate of reaction would be reduced where fusion occurred because diffusion through the slag film would become controlling. Similar results could be expected if internal melting occurred in the particles once sufficient carbon was removed. The sharp drop in the curves for particles in the 0.05–0.07 and 0.21–0.30 mm size range of Figure 9 probably indicates melting and the curve for the 0.5–0.59 mm size range and the curve for experiments at 1320°C for ground but not sieved coal minerals in Figure 10 shows sintering.

Feed and product particles from the experiments at 1320°C have been examined using the scanning electron microscope. The feed particles appear to contain specific mineral grains such as iron sulfide, alumina, silica, calcium carbonate, and kaolin clay encapsulated in a hard, nearly nonporous carbon matrix. Some small pores exist in the matrix, but pore size was less than 5 μm and represented less than 3% of the total volume of each particle.

The character of the solids within the particles after gasification indicated some fusion of the noncarbon fraction had occurred. Unfortunately, it was not possible to define the model precisely from the photomicrographs since intermediate particle samples were unobtainable.

The activation energy of the steam-carbon reaction can be calculated from the data obtained. A least-squares line from the intercept data for Kentucky No. 9 coal minerals gives

$$\ln k = \ln k_0 - \frac{E}{RT} = 1.52 - \frac{9974}{T} \qquad (19)$$

The value obtained from this work is 19.8 kcal/mol, to be compared with earlier work by Lowry (1963) on coal char which gave values ranging from 13.1 to 62.3. The reactivity is thus similar to that of a low-volatile char and the reaction rate could be expected to be slow and similar to that for coal gasification (Levenspiel, 1967).

These data indicate that the carbon–steam reaction is a slow, first-order, chemical reaction rate controlled process. Scott (1941) and Key et al. (1922) have suggested that the carbon–steam reaction is not first order with respect to carbon. Assuming that their carbon was similar in reactivity to the coal minerals, this conclusion appears incorrect. The shift reaction seems to be of little importance until late in the experiments, when the carbon available in the coal minerals has diminished and can no longer compete with the CO for the water in the reactor. These data agree with those of Gadsby et al. (1948). Haslam et al. (1923), and Key et al. (1930) using coal char carbons.

The gasification data coupled with the photomicrographs of coal mineral feed and gasifier product do not distinguish between the mathematical models which should be applicable to the process. Since the porosity of the feed particles is apparently quite small, the pore model proposed by Ishida and Wen (1971) should not apply except where sintering occurred, i.e., at 1320°C. Since no samples of particles were obtainable at intermediate reaction times, distinction between the general model, unreacted core shrinking model, and grain model was not possible without additional experimentation.

Conclusions

Coal mineral carbon can be successfully reacted with water in a fluid bed reactor to produce mixed hydrogen and carbon monoxide for use as fuel gas or hydrogenating medium. Pyritic sulfur is converted to hydrogen sulfide. The reaction temperature should be between 1100 and 1200°C to minimize CO_2 formation, have maximum carbon reactivity, and minimum melting of the coal minerals. The reaction is relatively slow and reaction rate-controlled and is substantially independent of particle size. The shrinking core model of Levenspiel (1967) as modified by Wen (1968) and Ishida et al. (1971) numerically represents the reaction until melting or sintering occurs within the bed. Firm conclusions should not be drawn as to the molecular mechanism pending experimental evidence capable of completely distinguishing between the mathematical models which may apply.

Nomenclature

a = stoichiometric coefficient

C_A = concentration of fluid reactant, C_A' in the reaction zone, C_{Ac} unreacted core surface, C_{Am} at the boundary between the reaction zone and diffusion zone, C_{Ao} in the bulk phase, C_{As} at the outer surface of the particle, mol/L^3

C_s = concentration of solid reactant, C_{so} initial concentration of solid reactant, mol/L^3

D_{eA} = effective diffusivity of fluid A in the ash layer, L^3/t

E = activation energy, H/m mol

k_{ma} = mass transfer coefficient across the fluid film, L/t

k_s = reactant rate constant based on surface, $L^{3(m+n-2)}/(\text{mol})^{m+n-1}t$

k_v = reaction rate constant based on volume, $L^{3(m+n-1)}/(\text{mol})^{m+n-1}t$

M_A = total reaction rate, mol/t

R_p = particle radius, L

R = gas constant, atm L^3/mol T

r_c = distance from particle center to reacting core, L

$\bar{r}_c$ = equivalent reaction radius for a particle surface defined by eq 18, L

r = distance from particle center, L

T = temperature

t = time

t_v = time of reaction, t

t_v^* = time for complete reaction, t

X = conversion

ϵ = voidage

$(n_s)_{\bar{r}_c}$ = effectiveness factor for surface reaction based on

Literature Cited

Chung, K. E., M.S. Thesis, Washington State University, Pullman, Wash., 1972.

Gadsby, J., Hinselwood, C. H., Sykes, K. W., *Proc. Roy. Soc. London, Ser. A*, **187**, 129 (1946).

Gadsby, J., *Proc. Roy. Soc. London, Ser. A*, **193**, 357 (1948).

Haslam, R. T., Hitchcock, F. L., Rudow, E. D., *Ind. Eng. Chem.*, **15**, 115 (1923).

Ishida, M., Wen, C. Y., *A.I.Ch.E. J.*, **14** (2), 311 (1968).

Ishida, M., Wen, C. Y., *Chem. Eng. Sci.*, **26**, 1031 (1971).

Ishida, M., Wen, C. Y., Shirai, T., *Chem. Eng. Sci.*, **26**, 1043 (1971).

Jensen, G. A., Monthly Letter Reports to the Pittsburg and Midway Coal Mining Company, 1968–1972.

Jensen, G. A., Ph.D. Thesis, Washington State University, Pullman, Wash., 1973.

Jones, C., *Anal. Chem.*, **39** (14), 1859 (1967).

Key, A., Cobb, J. W., *J. Soc. Chem. Ind.*, **49**, 439T (1930).

Kirk-Othmer, "Encyclopedia of Chemical Technology," 2nd ed, Vol. 12, Interscience, New York, N.Y., 1966.

Kloepper, D. L., Rogers, T. F., Wright, C. H., Bull, W. C., Office of Coal Research, The Department of the Interior, R & D Report No. 9 (December 1965).

Levenspiel, O., "Chemical Reaction Engineering," 2nd ed, Wiley, New York, N.Y., 1967.

Long, F. J., Sykes, K. W., *Proc. Roy. Soc. London, Ser. A*, **193**, 377 (1948).

Lowry, H. H., "Chemistry of Coal Utilization," Vol. 1, Wiley, New York, N.Y., 1947a.

Lowry, H. H., "Chemistry of Coal Utilization," Vol. 2, Wiley, New York, N.Y., 1947b.

Lowry, H. H., "Chemistry of Coal Utilization," Supplementary Volume, Wiley, New York, N.Y., 1963.

May, W. G., Mueller, R. H., Sweetster, S. B., *Ind. Eng. Chem.*, **50** (9), 1289 (1958).

Paxton, S., Cobb, J. W., *Gas J.*, **163**, 160 (1932); *World*, **78**, 619 (1963).

Purcell, J., Ettre, L. S., *J. Gas Chromatogr.*, **3**, 69 (1965).

Scott, G. S., *Ind. Eng. Chem.*, **33**, 1279 (1941).

Vohra, I. R., M.S. Thesis, Washington State University, Pullman, Wash., 1972.

Wen C. Y., *Ind. Eng. Chem.*, **60** (9), 34 (1968).

Wen, C. Y., Abraham, O. C., Talwalker, A. T., *Adv. Chem. Ser.*, **No. 69**, 253 (1962).

Received for review May 20, 1974
Accepted February 10, 1975